HHS Public Access

Author manuscript

Brain Struct Funct. Author manuscript; available in PMC 2016 September 01.

Published in final edited form as:

Brain Struct Funct. 2015 September ; 220(5): 2967–2982. doi:10.1007/s00429-014-0838-1.

Multiscale fingerprinting of neuronal functional connectivity

Gang Song, **Chung Tin**, and **Chi-Sang Poon***

Institute for Medical Engineering and Science, Massachusetts Institute of Technology, Cambridge, MA 02139, USA

SUMMARY

Current cellular-based connectomics approaches aim to delineate the functional or structural organizations of mammalian brain circuits through neuronal activity mapping and/or axonal tracing. To discern possible connectivity between functionally identified neurons in widely distributed brain circuits, reliable and efficient network-based approaches of cross-registering or cross-correlating such functional-structural data are essential. Here, a novel cross-correlation approach that exploits multiple timing-specific, response-specific and cell-specific neuronal characteristics as coincident fingerprint markers at the systems, network and cellular levels is proposed. Application of this multiscale temporal-cellular coincident fingerprinting assay to the respiratory central pattern generator network in rats revealed a descending excitatory pathway with characteristic activity pattern and projecting from a distinct neuronal population in pons to its counterparts in medulla that control the post-inspiratory phase of the respiratory rhythm important for normal breathing, airway protection and respiratory-vocalization coordination. This enabling neurotracing approach may prove valuable for functional connectivity mapping of other brain circuits.

Keywords

multiscale fingerprinting; functional connectivity; pneumotaxic center; Kölliker-Fuse nucleus; pons; post-inspiratory activity; respiratory rhythm; laryngeal motoneurons

INTRODUCTION

A fundamental question in neuroscience is how to explain brain behavior and function based on neuronal data. Currently, many methods exist to record or image central neurons extensively and to analyze their membrane and intracellular properties as well as overall afferent and efferent projections from and to other brain nuclei in great detail. Yet, how these neurons are wired together to form a functional circuit that simulates the underlying brain behavior and function remains largely unknown. Mapping *functional* connectivity (i.e., connectivity of functionally identified neurons) of mammalian brain circuits to elucidate the underlying system behaviors and physiological functions emergent from cellular and

*Corresponding author: Institute for Medical Engineering and Science, Bldg. E25-250, Massachusetts Institute of Technology, 77 Massachusetts Avenue, Cambridge, MA 02139, USA, Tel: +1 617-258-5405; Fax: +1 617-258-7906, cpoon@mit.edu.
Chung Tin's current address: Department of Mechanical and Biomedical Engineering, City University of Hong Kong, 83 Tat Chee Avenue, Hong Kong

subcellular properties is a major unmet challenge in brain research for which reliable probes of general applicability are presently lacking. Although dense local neural networks that are confined to a small volume may be reconstructed exhaustively with high-resolution and high-throughput imaging techniques such as automated volume electron microscopy in some cases (Helmstaedter 2013), discerning functional connectivity in widely distributed brain circuits remains an intractable task. Recent initiatives to address this challenging problem call for development of next-generation nanotechnology, multiphoton microscopy and optogenetics tools to continuously record and influence the firing patterns and sequences of every neuron (or a sizable fraction of the neurons) in a brain circuit along with next-generation very-large-scale neurocomputing tools for processing the resulting massive data and for building multiscale data-driven models on the mesoscale in order to analyze the underlying emergent principles (Abbott 2013; Alivisatos et al. 2013; Alivisatos et al. 2012; Devor et al. 2013). To learn how the function of a circuit follows from its structure, the resulting brain activity map is to be correlated with the measured *structural* connectivity (i.e., connectivity of anatomically identified neurons) of the circuit neuron-by-neuron in order to predict the overall behavioral or functional output. However, because brain activity maps are not anatomically labeled and structural connectivity maps are not functionally labeled, there is no way to correlate them directly. Thus, even when the activities of all neurons in a circuit are precisely recorded and their structural connectivity precisely imaged, functional connectivity of the circuit still cannot be derived until effective and reliable means of cross-registering or cross-correlating such cellular-based functional-structural data become available. Here, we propose a novel network-based neurotracing assay for this purpose (Fig. 1).

In the medulla, several neuronal populations with characteristic rhythmic discharge patterns that are synchronized to distinct phases [inspiratory, post-inspiratory (post-I) or early-expiratory (early-E), late-expiratory phase] (Richter et al. 1992) of the respiratory rhythm have been suggested to constitute the basic building blocks of a respiratory central pattern generator (rCPG) (Smith et al. 2013). The precise connectivity of this medullary rCPG network is presently unclear and various neural network models have been proposed to simulate certain physiological behaviors under specific test conditions (Shevtsova et al. 2011; Lindsey et al. 2012; Dutschmann and Dick 2012; Molkov et al. 2013; Smith et al. 2013). However, computer simulation is a necessary but not sufficient test of functional connectivity as many different connectivity patterns and model parameters could yield the same model output. In particular, recent evidence reveals that the post-I phase of the respiratory rhythm is dependent not only on medullary rCPG but also on descending drive from the Kölliker-Fuse nucleus (KFN) (Dutschmann and Herbert 2006), a core subdivision of the classic ‘pneumotaxic center’ in rostral dorsolateral pons whose function is known to be critically dependent on NMDA receptor (NMDAR) activity and is generally thought to promote inspiratory-expiratory phase transition (inspiratory off-switch) independent of vagal proprioceptive input (Dutschmann and Dick 2012). Post-I activity plays an important role in coordination of breathing movements with a variety of behavioral and defensive tasks involving laryngeal glottic closure such as vocalization, breath-holding (e.g., during diving or medical chest examination), airway protection during swallowing, coughing and sneezing, as well as expiratory braking to prevent premature lung emptying especially in

infants (Shiba 2010; Ludlow 2011; Dutschmann and Dick 2012; Subramanian 2013; Bautista and Dutschmann 2014). Abnormal expression of post-I activity may underlie laryngeal dysfunctions in certain neurological disorders such as Alzheimer's disease and Rett syndrome (Dutschmann et al. 2010; Dutschmann and Dick 2012; Stettner et al. 2007; Song et al. 2011) and may lead to laryngospasm or even life-threatening central apneas due to disease, prematurity, or high altitude (Stettner et al. 2008). Recent data have implicated the KFN/parabrachial complex as the site of respiratory-vocalization coordination although the neural substrate underlying such interaction is unclear (Smotherman et al. 2006). A critical question arising is whether this descending pneumotaxic post-I drive from KFN to the medullary rCPG network to modulate the respiratory rhythm is tonic (null hypothesis) or is rhythmic with respiratory phase modulation (alternative hypothesis). A tonic pneumotaxic drive that promotes post-I activity in the medulla would verify an exclusively medullary origin of the three-phase respiratory rhythm, with the pontine pneumotaxic center providing only a threshold-lowering drive for the inspiratory off-switch, as is traditionally held (Smith et al. 2007; Smith et al. 2013; von Euler 1977). In contrast, a respiratory phase-modulated pneumotaxic drive that is capable of gating the post-I phase would imply that the KFN is obligatory in whole or in part for the genesis of post-I activity.

To test these competing hypotheses, it is necessary to identify the origin of the descending pneumotaxic drive and its neuronal targets in the medullary rCPG. Among the various families of pontine respiratory-related neurons previously identified, a population of neurons (early-E neurons) has been observed to display rhythmic firing with a decrementing pattern during the post-I phase in both vagotomized (Cohen and Wang 1959; Song et al. 2006; Dutschmann and Herbert 2006; Dick et al. 1994) and vagal-intact animals (Ezure and Tanaka 2006). Pontine neurons with pure tonic firings are rare as they often exhibit subtle respiratory modulations (Cohen and Wang 1959; Dick et al. 1994; Song et al. 2006; Ezure and Tanaka 2006). One approach to testing which pontine neuronal population sends the descending pneumotaxic drive is by means of classical cross-correlation analysis of paired spike train recordings (or spike-triggered averaging of membrane potential sequences) from functionally identified pontine and medullary respiratory-related neurons (Kirkwood 1979; Hempel et al. 2002). However, because of the relative scarcity and heterogeneity of these neurons and the sparsity of such long-range connectivity, match-making specific neuronal pairs that are potentially connected in order to perform cross-correlation analysis is generally like finding a needle in a haystack and the experimental yield of this brute-force approach is bound to be low. Moreover, interpretation of cross-correlation spike train data or spike-triggered averaging data relies heavily on certain idealized assumptions on the underlying statistical model that may not always be valid in practice particularly when the recorded neurons are embedded in a larger interconnected network or the recorded spike trains are too short or have low firing rates. Such ambiguities make it difficult to discriminate with statistical confidence whether the observed correlated (or spike-triggered) activities stem from feedforward synaptic connectivity between the recorded neurons or from correlated common-mode inputs to both neurons or other extraneous factors, and whether failure to detect correlation reflects the lack of synaptic connectivity or insufficient statistical power or that the connectivity is just too weak (Ostojic et al. 2009; Pernice et al. 2011; Trousdale et al. 2012; de la Rocha et al. 2007). Not surprisingly, recent exhaustive

multielectrode/multisite spike train cross-correlation analyses of pontine and medullary respiratory-related neurons (n > 3,000) revealed only a paucity of possible pontomedullary functional links, at a detection rate for each purported link that was well within the false-positive statistical margin and a non-detection rate well within the false-negative statistical margin (Segers et al. 2008).

Rather than correlating spike-train activities, we propose a novel *multiscale temporal-cellular coincident fingerprinting* assay in which multiple timing-specific, response-specific and cell-specific neuronal characteristics that are consistently manifested at the cellular, network and systems levels are exploited as temporal-cellular coincident 'fingerprint markers' in order to verify functional connectivity between specific neuronal pools in a neural pathway (Fig. 1). Application of this network-based neurotracing assay allowed us to unequivocally identify an excitatory pontomedullary pathway from a distinct neuronal population in KFN to its counterparts in the medullary rCPG that control the post-I phase of the respiratory rhythm and modulate laryngeal adductor motor activity important for normal breathing, airway protection and vocalization. This finding provides the first demonstration of long-range functional connectivity of well-defined neuronal populations recorded from distinct brain nuclei subserving specific physiological functions at multiple levels of organization from cells to behavior. The results suggest a viable blueprint for mapping functional connectivity of other mammalian brain circuits.

METHODS

Experiments were conducted on 25 male adult Sprague-Dawley rats (300-350 g). Experimental protocols were as reviewed and approved by the M.I.T. Committee on Animal Care in accordance with published guidelines.

Animal preparation

Rats were anesthetized with urethane at initial dose of 1.5 g/kg (i.p.), paralyzed with pancuronium bromide (initial dose 0.5 mg, i.v., supplemented every hour at 0.1 mg, i.v.) and ventilated with hyperoxic medical air (O_2 enriched to 40%) by using a CWE AVS-1 ventilator. Supplemental doses of urethane (1/10 of initial dose, i.p. or i.v.) were given to maintain adequate anesthesia when noxious stimuli (e.g. clamping the tail or hind paw) evoked withdrawal response or changes in respiration and blood pressure. End-tidal CO_2 ($P_{ET}CO_2$ level was monitored (Capstar-100, CWE) and maintained at 5.0±0.2% (38±1.5 mmHg). Body temperature was kept at 36.5±0.5 °C with a temperature controller (TC-831, CWE). Atropine sulphate was injected (0.025 mg, s.c.) to reduce respiratory tract secretions. Trachea was cannulated for artificial ventilation. A femoral vein and artery were cannulated for infusing solution (Lactated Ringer's solution containing 5% glucose, 0.05-0.1 ml/min) or monitoring arterial blood pressure (BP-100, CWE, Ardmore, PA), respectively.

The head of the rat was fixed onto a stereotaxic frame (KOPF 1430, David Kopf Instruments, Tujunga, CA) in a tilted position with Bregma 1.5 mm higher than Lambda. Surgical procedures were as described previously (Song and Poon 2009). Briefly, a phrenic nerve and both cervical vagus nerves were isolated, cut, and exposed from a dorsal

approach. An occipital craniotomy was performed at interaural level to expose brain surface for implanting stimulation/recording electrode or microinjection pipette.

The central cut-ends of phrenic or vagus nerves were mounted on bipolar platinum wire recording electrodes. The raw phrenic or vagal motor discharges were amplified (CyberAmp 380, Axon Instruments, Union City) and sampled (at 10 KHz) into a Dell PC with LabView (National Instruments, Austin, TX). The raw signals were also integrated with an analog Paynter filter (time constant 50 ms) or digitally with custom-made MATLAB software (MathWorks, Natick, MA) at a time constant of 25 or 50 ms.

Hypoxia test

Hypoxia was applied by switching the ventilation gas from hyperoxic (40% O_2) medical air to a hypoxic (8% O_2 balance N_2) gas. The hypoxia test consisted in 1 min of pre-test baseline recording, 30 or 50 sec of hypoxia, and 8 min of post-hypoxia recovery. The gas flow rate was carefully controlled so that ventilation remained unchanged throughout the entire experiment. In some rats, hypoxia tests were performed both before and after microinjection of neurochemicals into the KFN. After microinjection, the animals were allowed to stabilize for 3-5 min before another hypoxia test was given.

Microinjection of AP5 into intermediate KFN

Microinjection of AP5 was delivered by a micropipette at a locus within KFN in which electrical or chemical stimulation produced characteristic responses in vagal and phrenic motor discharges as described by Dutschmann and Herbert (Dutschmann and Herbert 2006) (Fig. S1A-D, Supplemental Data). Briefly, a monopolar tungsten microelectrode (tip diameter 1-2 μm, impedance 0.5 MΩ; Micro Probes, Gaithersburg, MD) was inserted stereotaxically into KFN at mediolateral coordinates of 2.3 - 2.6 mm lateral to midline, rostrocaudal coordinates of +0.2 - - 0.2 mm to interaural level, and dorsoventral coordinates (depths) of 8.0 - 8.5 mm from lambda surface (Paxinos et al. 1999; Paxinos and Watson 1986). Electrical stimulation was delivered through an isolator (A.M.P.I. ISO-Flex) at an intensity of 20-40 μA, pulse duration of 0.3 ms and frequency of 100 Hz. After the intermediate KFN was identified, the stimulation electrode was withdrawn and a microinjection pipette was inserted to the same locus. The microinjection pipette (tip diameter 15-30 μm) was pulled from Borosilicate glass pipette (O.D. 1 mm, I.D. 0.5 mm) and filled with AP5 (5 mM in ACSF, Sigma, St. Louis, MO). Injection (25-50 nl) was performed by applying pressure pulses (10 Psig, pulse duration 0.1-0.3 sec) to the pipette using a microinjector (BH2, Harvard Apparatus, Holliston, MA).

Unit recording and local picoinjection

Respiratory-related neuronal unit discharge in KFN (at coordinates as described above) and the ventral medullary respiratory column (1.8-2.2 mm lateral from midline, 0-2 mm rostral to obex, depth 2.5-3 mm from dorsal brainstem surface) spanning the Bötzinger complex, preBötzinger complex, and ventral respiratory group was recorded with a stereotaxically inserted Carbostar-1 carbon fiber microelectrode (Kation Scientific, Minneapolis, MN) or glass micropipette (pulled from O.D. 1.2 mm Borosilicate glass pipette and filled with 0.5 M NaCl, impedance 15-20 MΩ). Unit discharge was amplified (AxoClamp 2B, Axon

Instruments, Union City) and sampled into a computer with LabView software at a sampling rate of 10 KHz.

Some units in KFN were recorded with Carbostar-3 multibarrel microelectrode (Kation Scientific). The central barrel of this microelectrode (imbedded with a carbon microfiber) was used for extracellular unit recording. Side-barrels were connected to a microinjector. One side-barrel was filled with AP5 solution (5 mM in ACSF, Sigma). The other side-barrel was filled with bicuculline solution (5 mM in ACSF, Sigma) or with ACSF for control injection. To estimate the volume of injection, test-injections were performed while the tip of the multibarrel microelectrode was exposed in air. With our experimental setup, a pulse pressure of 10 Psig (pulse duration of 0.1 sec) produced a droplet with diameter of 20-30 μm (volume estimated to be 4-14 picoliter) at the tip of the microelectrode. Upon the recording of unit discharge, picoinjection was made to this unit by applying the same pressure pulse.

Histology

At the end of the experiment, the loci of microinjection and unit recording were marked by making small electrolytic lesions (D.C. +100 μA, 30 sec). The animal was euthanized by urethane overdose and perfused with paraformaldehyde solution (4% in 0.01 M PBS). The brain was removed, post-fixed and cut into 100-μm coronal or sagittal sections on a freezing microtome (Leica, SM2010R, Buffalo Grove) for microscopic identification of the injection or recording loci. Figure S1E (Supplemental Data) shows an example of the microinjection site.

Immunohistology and retrograde neural tracing

Three additional rats were studied for neuronal projections from KFN to the Bötzinger complex using retrograde neural tracing and immunohistology (double labeling). The rat was anesthetized with pentobarbital (initial dose 60 mg /kg, i.p., supplemental dose 1/10 of initial dose) until surgical analgesia was reached (no response to paw clamp). The rat's head was fixed in a stereotaxic frame (KOPF 1430, David Kopf Instrument, Tujunga, CA) and flexed 30° downward and the atlanto-occipital foramen was exposed by cutting open the overlying skin and separating the muscles. Then the dura at the atlanto-occipital foramen was removed and part of the occipital bone cut-off to expose the dorsal medulla surface. The Bötzinger complex was stereotaxically located (1.8-2.2 mm lateral from midline, 1.6-2 mm rostral from calamus scriptorius, at depth of 2.7-3.0 mm from dorsal medulla surface) and confirmed by the recording of post-I or augmenting expiratory neuronal discharges. Then a glass micropipette (tip diameter 15-30 μm) filled with retrograde tracer RetroBeads ™ (Lumafluor Inc.) was inserted into the Bötzinger complex and a volume of 30-60 nl was pressure-injected.

After microinjection, the surgical wound was cleaned and sutured. The rat was given Buprenex (0.03 mg/kg, s.c., b.i.d.), Meloxicam (1 mg/kg, s.c., daily), and Ringer's solution (10-20 ml, s.c.) when necessary. Three to five days after the injection, the animal was euthanized with pentobarbital (100 mg/kg, i.p.) and transcardially perfused with PBS and paraformaldehyde. The brainstem was removed, post-fixed and cut into sequential 50-μm coronal sections on a freezing microtome. Brainstem sections of rostral pons were processed

for immunefluorescent visualization of NMDA receptor subunit R1 (NR1). Briefly, the sections were incubated in rabbit monoclonal anti-NR1 antibody (Millipore Cat # AB9864, RRID: AB_2112158, at 1:200 dilution in PBS containing 0.3% Triton X-100 and 3% goat serum) for 48 hours at 4°C, rinsed, and then in goat anti-rabbit IgG (Alexa Fluor-488 conjugated, A11008, Invitrogen-Life Science, at 1:500 dilution) for 2 hours at room temperature. Sections were rinsed again, mounted unto slides, dried and coverslipped. For control purpose, another set of brainstem sections were processed with the same method as described above except that the rabbit anti-NR1 was omitted. Sections were observed under fluorescent microscope (Zeiss fluorescent Axio microscope, Carl Ziss MicroImaging, LLC), photographed with Axiocam (Zeiss) and analyzed with AV Rel 4.8.2 software (Zeiss).

Data analyses

As shown in Fig. S2, the amplitude of phrenic discharge, inspiratory and expiratory durations (T_I, T_E) and respiratory frequency (f) were measured for each respiratory cycle from integrated phrenic discharge ($\int$ phr). The amplitude of vagal post-I discharge ($\int$ vagal post-I amplitude) was measured as the peak amplitude of the integrated vagus curve ($\int$ vagus) at the beginning of the post-I phase. Duration of the post-I phase or stage I expiration (T_{E1}) was measured as the duration of vagal post-I discharge (from the end point of T_I to the minimum point of the $\int$ vagus curve) and duration of late-E phase or stage II expiration (T_{E2}) as T_E minus T_{E1}. We also calculated the area of integrated vagal discharge during the post-I phase (area under the $\int$ vagus curve of post-I phase, the shaded area in Fig. S2) as a surrogate for T_{E1} in cases where post-I activity was weak and T_{E1} could not be reliably estimated. Discharges of KFN early-E units were counted for each expiratory phase as a measure of neuronal activity. The unit discharges were also converted to time-stamp signals and plotted into perievent histograms against the inspiratory/expiratory event markers extracted from phrenic discharges using commercial software (OfflineSorter, Plexon, Dallas, TX; NeuroExplorer, Nex Technologies, Littleton, MA), as described previously (Song et al. 2006).

Statistical analysis

All measured values were normalized against corresponding pre-hypoxia baseline values in control or post-microinjection conditions, and averaged every 10 seconds. Each animal served as its own control for all statistical analyses. All analyzed values are expressed as means ± SE. Student *t* test and ANOVA (one-way or two-way ANOVA with repeated measures followed by Tukey post-hoc analysis) were used to determine statistical significance. Confidence level of 95% was used.

RESULTS

Temporal-cellular coincident fingerprinting of post-I pathway at systems level

First, we sought to define a set of temporal and cellular markers of the post-I pathway as manifested at the systems level in vagotomized rats that would constitute a sufficient basis for fingerprinting the pathway at the network and cellular levels (Fig. 1). We hypothesized that the pontine pneumotaxic mechanism's unique property of critical dependence on NMDAR activity (reviewed in (Poon and Song 2014; Dutschmann and Dick 2012)) may

provide a cell-specific marker of the pontomedullary post-I pathway. This is in contrast to other central neurons in which excitatory transmission is typically mediated by both NMDA and AMPA channels so that neuronal firing is depressed but not abolished by NMDAR blockade alone (Krolo et al. 1999; Zhou et al. 1997). For a timing-specific and response-specific temporal-cellular markers, we used a hypoxia test to evoke changes in the respiratory rhythm, in part through excitation of a peripheral chemoafferent pathway that projects to KFN (Song et al. 2011). We found that a brief period of hypoxic chemoreceptor stimulation (8% O_2 in inspired gas for 50 sec) induced short-term potentiation (STP) of the post-I phase as evidenced by abrupt post-hypoxic increases in the amplitude and duration of vagal post-I motor activity (as a surrogate for laryngeal adductor motor activity (Dutschmann and Herbert 2006)) (Figs. 2A, 2C1, 2C2). Microinjection of the NMDAR antagonist AP5 into an intermediate area in KFN (Fig. 2D and Fig. S1, Supplemental Data) markedly diminished the amplitude and duration (T_{E1}) of vagal-laryngeal post-I motor activity and abolished their post-hypoxic STP (Figs. 2B, 2C1) indicating that the NMDAR-dependent pneumotaxic mechanism in KFN contributed importantly to the emergence of the post-I phase and its post-hypoxic STP. In contrast, the hypoxic stimulus did not induce STP of the late-expiratory phase (Fig. 2C2; see definition of late-expiratory phase in Fig. S2, Supplemental Data) and blockade of NMDAR activity in KFN did not abolish the late-expiratory phase and T_{E2} (Fig. 2B) or inspiratory phase and T_I (Figs. 2B, 2C3). These data suggest that post-hypoxic STP of the post-I phase was a timing-specific and response-specific property of the NMDAR-dependent pneumotaxic mechanism in KFN that was independent of the other phases of the respiratory rhythm. Hence, post-hypoxic NMDAR-dependent STP of the post-I phase constituted a sufficient set of timing-specific (criterion 1), response-specific (criterion 2), and cell-specific (criterion 3) markers for coincident fingerprinting of the pontomedullary post-I pathway (Fig. 1).

Temporal-cellular coincident fingerprinting of post-I pathway at network level

The data in Figs. 2 at the systems level suggest that the NMDAR-dependent pneumotaxic drive from KFN phase-selectively facilitated post-I motoneuron activity. To investigate whether medullary post-I interneurons were also selectively facilitated by NMDAR-dependent pneumotaxic drive from KFN at the network level, we analyzed the activities of various medullary respiratory-related neurons. Brief hypoxic stimulation induced post-hypoxic STP of all post-I interneurons (n = 10) and a post-I motoneuron (n = 1) recorded from the ventrolateral medullary respiratory column (Fig. 3D), as evidenced by post-hypoxic increases in the discharge frequency and duration of these neurons in the post-I phase (Figs. 3A, 3B) similar to those exhibited by vagal efferent nerve discharge (Figs. 2A, 2C1, 2C2). After microinjection of AP5 at KFN bilaterally, all the recorded post-I neurons were markedly depressed or completely silenced and their post-hypoxic STP was greatly diminished or abolished (Figs. 3A, 3B).

Concordant with the abolition of the post-I phase after NMDAR blockade at bilateral KFN, the discharge of medullary late-expiratory neurons (expiratory-augmenting; n = 3) now spanned the entire expiratory phase (Fig. 3C). The discharge patterns of various medullary inspiratory neurons (n = 10) were not significantly altered although their firing frequencies were slightly or moderately reduced (Fig. 3C). These observations at the network level

corroborate the inference from data at the systems level (Fig. 2) that medullary post-I interneurons and motoneurons were targeted by descending excitatory drive from NMDAR-dependent KFN pneumotaxic neurons.

Consistent with this result, Fig. 3E shows that many neurons in rat KFN that were immunopositive to the NMDAR subunit R1 (NR1) could be retrogradely labeled with fluorescent microspheres (RetroBeads ™, Lumafluor) microinjected into the Bötzinger complex, a key respiratory-related area in the ventrolateral medulla where many post-I neurons are known to be localized [reviewed in (Poon and Song 2014)]. Careful examination of the RetroBeads ™ and NR1 double-labeled neurons vs. RetroBeads ™ single-labeled neurons revealed that the majority (estimated to be >90% from representative sections) of neurons in KFN that sent axonal projections to the Bötzinger complex expressed NR1, indicating monosynaptic modulation of Bötzinger complex neurons by NMDAR-dependent KFN neurons.

Temporal-cellular coincident fingerprinting of post-I pathway at cellular level

The foregoing results at the systems and network levels indicate that the KFN pneumotaxic drive: (i) selectively targeted medullary post-I neurons to facilitate the post-I phase and laryngeal adductor motor activity (timing-specific criterion); (ii) exhibited post-hypoxic STP in facilitating the amplitude and duration of post-I activity (response-specific criterion); and (iii) was abolished by NMDAR blockade (cell-specific criterion). Such post-I phase selective and NMDAR-dependent STP characteristics (criteria 1-3) provided a sufficient set of timing-specific, response-specific and cell-specific coincident fingerprint markers for identifying the neural correlate of the KFN pneumotaxic mechanism (Fig. 1). From (i), it follows that the pneumotaxic drive from KFN to medullary post-I neurons would be unlikely to be tonic or phase-spanning with a significant inspiratory or late-expiratory component, since activation of medullary post-I interneurons beyond the post-I phase would likely impact other respiratory phases through their inhibitory actions on other respiratory-related neurons [reviewed in (Poon and Song 2014)]. Indeed, none of the tonic neurons we recorded from KFN (n = 46) were responsive to hypoxic stimulus or demonstrated post-hypoxic STP, in violation of criterion (ii) (Fig. 4). Thus, the conventional null hypothesis of a tonic descending pneumotaxic drive from KFN to the medullary rCPG was not supported by these data.

In contrast, consistent with criterion (i) early-E neurons recorded from KFN were active mainly during the post-I phase with a decrementing discharge pattern (Fig. 5A, 5B). Post-experimental histology showed that the loci of the recorded early-E neurons were localized mostly in areas corresponding to the intermediate KFN as defined in Fig. S1 (Supplemental Data). The discharge of all these neurons (n = 15) in the post-I phase was depressed during hypoxia initially but exhibited rebound STP at the cessation of hypoxia (Fig. 5A-5C), whereas the discharge (if any) in the inspiratory phase remained minimal and was not recruited by hypoxia (Fig. 5C). Peri-event histogram analysis showed that the initial depression of neuronal activity during hypoxia was due to a decrease in the number of spikes/cycle rather than a decrease in peak instantaneous firing frequency (Fig. 5B). The time course of the responses in total discharge and mean firing frequency of these neurons

paralleled those of expiratory duration (Fig. 5D, 5E) such that their total discharge correlated linearly with expiratory duration (Fig. 5F). In another series of experiment (n=7), linear correlations were observed between early-E neuron discharge and integrated vagal-laryngeal post-I motor discharge during and after hypoxia (Fig. 5G, 5H) indicating that KFN early-E neuron activity was akin to post-I activity.

Having passed criteria (i) and (ii) for timing- and response-specific temporal-cellular markers above, we tested whether KFN early-E neurons also met criterion (iii) for cell-specific marker of the pneumotaxic mechanism. In KFN early-E neurons that were recorded using a multibarrel electrode, local picoinjection of AP5 directly at the neurons attenuated the post-hypoxic STP of the early-E neuronal discharges (Fig. 6). This was apparently secondary to a depression of baseline discharges by AP5 (Fig. 6A, 6B), such that when the neuron was silenced by AP5 its post-hypoxic STP was also abolished (Fig. 6C). Thus, KFN early-E neurons indeed exhibited post-hypoxic STP that was critically dependent on NMDAR activity.

DISCUSSION

The foregoing results demonstrate the applicability of the multiscale temporal-cellular coincident fingerprinting assay depicted in Fig. 1 in identifying the functional connectivity of a long-range pontomedullary post-I pathway. The consistent manifestation of coincident time-specific, response-specific and cell-specific markers [criteria (i)-(iii)] at the systems (Figs. 2), network (Figs. 3) and cellular levels (Figs. 4-6) unequivocally identified KFN early-E neurons as the neural correlate of the pontine pneumotaxic mechanism and medullary post-I interneurons and motoneurons as targets of the descending pontine pneumotaxic drive. The post-I interneurons are presumably inhibitory and glycinergic (Ezure et al. 2003); glutamatergic post-I neurons in the ventrolateral medulla have not been reported (reviewed in (Poon and Song 2014)). Our data suggest that this descending pathway is excitatory, as indicated by the post-hypoxic STP in the firing frequency of the post-I neurons. This conclusion is supported by previous neurotracing studies which showed that neuronal projections from KFN to medulla and spinal cord are glutamatergic (Yokota et al. 2011; Yokota et al. 2007; Yokota et al. 2004). Collectively, these data reveal an excitatory pontomedullary pathway from KFN early-E neurons to medullary post-I interneurons and motoneurons that plays a critical role in controlling the post-I phase of the respiratory rhythm and modulating vagal-laryngeal post-I motor activity.

A new paradigm for functional connectivity mapping of brain circuits

Mapping functional connectivity of brain circuits is a fundamental neurotechnological challenge that has severely hampered progress in brain research in the past. The crux of the problem lies in the fact that traditional cellular-based neurotracing techniques such as neuronal labeling, axonal tracing or optogenetic perturbation are generally inadequate for functional connectivity mapping at the network level, whereas high-resolution network imaging techniques such as automated volume electron microscopy (Helmstaedter 2013) are cost- and computation-prohibitive and are not scalable. Large-scale neuronal recordings for building the brain activity map, while important for resolving the high-dimensional

information encoding in certain complex brain systems (such as vision), may not guarantee functional connectivity mapping even for relatively small brain circuits such as the rCPG network. Indeed, the limitations of traditional spike-based cross-correlation analyses (see Introduction) preclude construction of the functional connectivity map directly from a brain activity map even when all neuronal spike trains are exhaustively recorded. Constructing the functional connectivity map by matching a brain activity map to corresponding structural connectivity map is equally difficult as it requires the neuronal activity data to be precisely cross-registered with axonal projection data neuron-by-neuron, which could be a major technological challenge by itself.

Another critical issue in the current debate about functional connectomics approaches is at what granularity should brain activity maps be realistically drawn that would ensure satisfactory prediction of brain behavior and function without oversampling? Because mammalian brain circuits are built with cell-type-specific neuronal populations each of which comprises a large number of neurons of similar functional type connected in parallel with a high degree of redundancy (unlike in lower invertebrates where every single neuron is unique and plays a critical role in determining brain function and animal survival), it may be more tractable experimentally and computationally to analyze the ensemble activity of neurons of similar functional types rather than exhaustively sampling all neurons in a circuit. Furthermore, the functional and structural similarities of neurons within the same population and their likely proximity to one another make it extremely difficult or impossible to selectively excite or suppress every neuron individually without affecting wholesale other similarly-situated neurons in the same population; hence, one can at best selectively manipulate the activity of each cell-type-specific neuronal population collectively one at a time. These fundamental constraints imply that the functional connectivity map of a brain circuit may realistically be constructed from its activity map only at a granularity generally no smaller than the population neurons level – rather than single-neuron level as originally envisioned (Alivisatos et al. 2012). Accordingly, a recently proposed consensus roadmap which is deemed realizable within a decade for relating neuronal activity to brain behavior and function calls for experimental manipulations and measurements of the ensemble activities of cell-type-specific neuronal populations instead of the activities of single neurons as the building blocks for computational modeling (Devor et al. 2013). However, connecting the dots of a brain activity map of any granularity before and after experimental perturbations is by no means trivial and calls for a rigorous conceptual framework to ensure the reliability and uniqueness of the resultant functional connectivity map and facilitate its efficient reconstruction from experimental data. The present study suggests a viable and readily applicable blueprint which may fill in this missing link.

In keeping with the suggested consensus roadmap (Devor et al. 2013), the present study also employed neuronal manipulations (sequential excitation/suppression) and measurements at the population neurons level but the proposed multiscale temporal-cellular coincident fingerprinting assay (Fig. 1) afforded much more well-defined and highly efficient mapping of functional connectivity for computational modeling of brain circuits than hitherto feasible. To understand how this works, it is important to recognize that a key requirement in functional connectivity inference from neuronal activity mapping is that any experimental manipulations of neuronal activity in order to discern the corresponding connectivity must

single out only the neurons of interest and not others. This requirement is highly challenging because it is generally difficult (if not impossible) to isolate cellular markers that are unique to a single neuronal population (let alone single neuron) for selective stimulation or suppression of that neuronal population alone with proven 100% specificity. To overcome this difficulty, we employ multiple cell-specific, timing-specific and response-specific markers to verify causality of the corresponding stimulus-response pathway at the neuronal, network and systems levels. The temporal characteristics of the timing-specific and response-specific markers add a new dimension for identifying neuronal connectivity in addition to the cellular signatures of the cell-specific and response-specific markers. Although each temporal-cellular marker (e.g. the NMDAR marker) may not be 100% specific to the neurons of interest, their coincidence forms a unique ‘fingerprint’ that can be consistently verified at the neuronal, network and systems levels to confirm functional connectivity with a high degree of confidence. This multiscale fingerprint provides a critical linchpin that effectively links the presynaptic and postsynaptic neuronal pools together. The choice of suitable temporal-cellular markers for unique fingerprinting may vary for different brain circuits depending on the characteristics of the pre- and postsynaptic neurons of interest, hence the corresponding experimental design may call for different neuronal manipulations than those illustrated in Fig. 1. Also, functional connectivities inferred from such experimental manipulations could be oligosynaptic, hence separate tests (e.g. Fig. 3E) may be necessary to verify monosynaptic connections as necessary.

To our knowledge, the present study represents the first successful mapping of long-range functional connectivity of a central neural pathway that is embedded in a larger interconnected network, circumventing the limitations of conventional spike-timing analyses. In contrast to structural connectivity mapping, which traces the connection between neurons whose anatomic locations and/or cellular properties are identified, our method traces the connection between neurons whose activity patterns are identified. This novel network-based neurotracing assay should be generally applicable to other brain circuits in the future to greatly accelerate functional connectivity mapping at any level of granularity depending on the available methods of neuronal activities measurement and experimental manipulation. In some brain circuits it may be possible to derive exogenous timing-specific and response-specific markers from patterned optogenetic excitation/inhibition of presynaptic neuron populations with cell-specific markers that allow for optogenetic manipulation. For example, the method of projection targeting uses optogenetic manipulation of a neuronal population to verify structural connectivity to their projection targets (Yizhar et al. 2011). For detailed functional connectivity mapping using multiscale fingerprinting in conjunction with projection targeting, activities of postsynaptic neuron populations must be recorded to verify the presence of similar cell-specific, timing-specific and response-specific markers at the network level that resemble those resulting from optogenetic manipulation of given presynaptic neuron population at the cellular level as depicted in Fig. 1.

Physiological, behavioral and translational implications of the newly identified pontomedullary post-inspiratory pathway

Our mapping of the functional connectivity of a pontomedullary excitatory pathway from KFN early-E neurons in pons to post-I neurons in medulla opens a new paradigm for understanding respiratory rhythm generation and respiratory control at the network and systems levels. Until now, it has been widely assumed that the mammalian respiratory rhythm arises from a core rCPG network that is localized within the medulla, with the pons providing only a tonic pneumotaxic input or recurrent feedback via efference copies (Dutschmann and Herbert 2006; Smith et al. 2013; Lindsey et al. 2012; Molkov et al. 2013; Dutschmann and Dick 2012). On the contrary, our application of the fingerprinting assay as depicted in Fig. 1 demonstrated that a functionally and anatomically defined population of early-E neurons in pons is the prime driver of normal post-I activity. The successful isolation of this neuronal population as the neural correlate of the pontine pneumotaxic mechanism and tracing of its excitatory connectivity to its counterparts in medulla represent a significant milestone in elucidating the pontine contribution to respiratory rhythm generation in the past nine decades since Lumsden (1923). Because KFN neurons send collateral projections to multiple respiratory-related regions in the medulla (Song et al. 2012), it is possible that these early-E neurons in KFN may excite multiple post-I interneurons and motoneurons which are widespread in the ventrolateral medullary respiratory column (Ezure et al. 2003).It is presently unclear how these early-E neurons in KFN generate their rhythm and unique post-I firing pattern; possible scenarios include emergent network properties through interaction with other pontomedullary respiratory neurons (Segers et al. 1985; Wang et al. 2008) or intrinsic cellular properties (e.g., pacemakers). Also unclear are the cellular mechanisms underlying the NMDAR-dependent STP in these early-E neurons. Such NMDAR-dependent STP of post-I activity and resultant prolongation of TE induced by hypoxic chemoafferent input may be homologous to the previously reported NMDAR-dependent short-term depression (STD) of the Hering-Breuer reflex prolongation of TE induced by vagal proprioceptive input (Siniaia et al. 2000; MacDonald et al. 2009; Song et al. 2011), as suggested recently (Poon and Song 2014). Further studies will be needed to address these issues in the future.

In addition, our identification of a specific neuronal population in pons that controls laryngeal glottic closure opens a new window for understanding how respiratory movements may be coordinated with a variety of respiratory-related physiological, behavioral and defensive tasks in health and the failure of such coordination in disease. Airway protection through glottic closure is phylogenetically the oldest and the most important function of the laryngeal adductor muscles that is critical for animal survival (Hoh 2010). Repetitive breath-holding due to involuntary glottic closure is a major cause of life-threatening apnea in preterm infants (te Pas et al. 2009; Martin and Wilson 2012) or post-anesthesia laryngospasm (Hampson-Evans et al. 2008) and a cardinal symptom of Rett syndrome (Stettner et al. 2007; Weese-Mayer et al. 2006). Additionally, aspiration pneumonia due to impaired glottic closure during swallowing is a major cause of death in many neurological disorders such as Alzheimer’s disease, intoxication, dysphagia, and stroke (Pitts 2013). All these dysfunctions have been attributed to abnormalities of the laryngeal adductor reflex presumably mediated by respiratory-related neurons in the medulla. In contrast, the present

results show that laryngeal adductor motor activity is directly controlled by early-E neurons in KFN, a pontine nucleus that is known to integrate ascending visceral afferent inputs with descending forebrain inputs and is hyperactive in Rett syndrome mutant mice (Stettner et al. 2007; Dutschmann and Dick 2012). This finding suggests a new cellular target for potential treatment of a variety of glottic closure dysfunctions in future.

Besides subserving respiratory and airway protection functions, the larynx (voice box) is the principal organ for voice production in mammals. All forms of vocalization (crying, laughing, speech, singing, sighing, coughing) except snoring occur during or immediately following the post-I phase of the respiratory rhythm with controlled expiratory airflow through the vocal cords. During voicing for speech, the vocal folds are constantly closing and contacting each other with each vibrating at ~120 Hz in men and >200 Hz in women (Ludlow 2011; Maltby et al. 2010). In bats (a vocally highly developed mammalian species), the vocal frequency could be >200 kHz and may be up-/down-regulated dynamically to compensate for flight-induced Doppler shifts in the echoes for navigation and foraging (Smotherman et al. 2003; Maltby et al. 2010). Therefore, precise dynamic control of laryngeal adduction in synchrony with the post-I phase of the respiratory rhythm is crucial for producing proper vocal pitch. Recent data have implicated the KFN/parabrachial complex in pons as an important site of respiratory-vocalization coordination (Smotherman et al. 2006; Smotherman et al. 2010). The present functional connectivity data identify KFN early-E neurons as the likely pontine neural correlate of respiratory-vocalization coordination.

In conclusion, our multiscale temporal-cellular coincident fingerprinting assay (Fig. 1) has unequivocally identified KFN early-E neurons as the neural correlate of the putative pontine pneumotaxic mechanism that is essential for the genesis of the post-I phase of the normal respiratory rhythm and for proper coordination of respiratory movements with vocalization and airway protection. These findings have far-reaching physiological, behavioral and translational implications. This enabling neurotracing assay may prove valuable for future systematic mapping of the complete functional connectivity of the pontomedullary rCPG as well as other brain circuits in general.

Supplementary Material

Refer to Web version on PubMed Central for supplementary material.

Acknowledgments

We thank Drs. J. Champagnat, G. Fortin, P.G. Guyenet, and D. Richter for valuable comments on an early version of the manuscript. This work was supported by National Institutes of Health grants HL067966 and HL093225.

References

Abbott A. Solving the brain. Nature. 2013; 499(7458):272–274. [PubMed: 23868244]

Alivisatos AP, Andrews AM, Boyden ES, Chun M, Church GM, Deisseroth K, Donoghue JP, Fraser SE, Lippincott-Schwartz J, Looger LL, Masmanidis S, McEuen PL, Nurmikko AV, Park H, Peterka DS, Reid C, Roukes ML, Scherer A, Schnitzer M, Sejnowski TJ, Shepard KL, Tsao D, Turrigiano

G, Weiss PS, Xu C, Yuste R, Zhuang X. Nanotools for neuroscience and brain activity mapping. ACS Nano. 2013; 7(3):1850–1866.10.1021/nn4012847 [PubMed: 23514423]

Alivisatos AP, Chun M, Church GM, Greenspan RJ, Roukes ML, Yuste R. The brain activity map project and the challenge of functional connectomics. Neuron. 2012; 74(6):970–974.10.1016/j.neuron.2012.06.006 [PubMed: 22726828]

Bautista TG, Dutschmann M. Ponto-medullary nuclei involved in the generation of sequential pharyngeal swallowing and concomitant protective laryngeal adduction in situ. J Physiol. 201410.1113/jphysiol.2014.272468

Cohen MI, Wang SC. Respiratory neuronal activity in pons of cat. J Neurophysiol. 1959; 22(1):33–50. [PubMed: 13621254]

de la Rocha J, Doiron B, Shea-Brown E, Josic K, Reyes A. Correlation between neural spike trains increases with firing rate. Nature. 2007; 448(7155):802–806.10.1038/nature06028 [PubMed: 17700699]

Devor A, Bandettini PA, Boas DA, Bower JM, Buxton RB, Cohen LB, Dale AM, Einevoll GT, Fox PT, Franceschini MA, Friston KJ, Fujimoto JG, Geyer MA, Greenberg JH, Halgren E, Hamalainen MS, Helmchen F, Hyman BT, Jasanoff A, Jernigan TL, Judd LL, Kim SG, Kleinfeld D, Kopell NJ, Kutas M, Kwong KK, Larkum ME, Lo EH, Magistretti PJ, Mandeville JB, Masliah E, Mitra PP, Mobley WC, Moskowitz MA, Nimmerjahn A, Reynolds JH, Rosen BR, Salzberg BM, Schaffer CB, Silva GA, So PT, Spitzer NC, Tootell RB, Van Essen DC, Vanduffel W, Vinogradov SA, Wald LL, Wang LV, Weber B, Yodh AG. The challenge of connecting the dots in the B.R.A.I.N. Neuron. 2013; 80(2):270–274.10.1016/j.neuron.2013.09.008 [PubMed: 24139032]

Dick TE, Bellingham MC, Richter DW. Pontine respiratory neurons in anesthetized cats. Brain Res. 1994; 636(2):259–269. [PubMed: 8012810]

Dutschmann M, Dick TE. Pontine mechanisms of respiratory control. Compr Physiol. 2012; 2(4):2443–2469.10.1002/cphy.c100015 [PubMed: 23720253]

Dutschmann M, Herbert H. The Kolliker-Fuse nucleus gates the postinspiratory phase of the respiratory cycle to control inspiratory off-switch and upper airway resistance in rat. Eur J Neurosci. 2006; 24(4):1071–1084. [PubMed: 16930433]

Dutschmann M, Menuet C, Stettner GM, Gestreau C, Borghgraef P, Devijver H, Gielis L, Hilaire G, Van Leuven F. Upper airway dysfunction of Tau-P301L mice correlates with tauopathy in midbrain and ponto-medullary brainstem nuclei. J Neurosci. 2010; 30(5):1810–1821.10.1523/JNEUROSCI.5261-09.2010 [PubMed: 20130190]

Ezure K, Tanaka I. Distribution and medullary projection of respiratory neurons in the dorsolateral pons of the rat. Neuroscience. 2006; 141(2):1011–1023.10.1016/j.neuroscience.2006.04.020 [PubMed: 16725272]

Ezure K, Tanaka I, Kondo M. Glycine is used as a transmitter by decrementing expiratory neurons of the ventrolateral medulla in the rat. Journal of Neuroscience. 2003; 23(26):8941–8948. [PubMed: 14523096]

Hampson-Evans D, Morgan P, Farrar M. Pediatric laryngospasm. PaediatrAnaesth. 2008; 18(4):303–307.10.1111/j.1460-9592.2008.02446.x

Helmstaedter M. Cellular-resolution connectomics: challenges of dense neural circuit reconstruction. Nat Methods. 2013; 10(6):501–507.10.1038/nmeth.2476 [PubMed: 23722209]

Hempel CM, Sugino K, Nelson SB. Multi-unit spike-triggered averaging: a method for probing the physiology of central synapses. J Neurosci Methods. 2002; 120(2):121–129. [PubMed: 12385762]

Hoh JFY. Laryngeal muscles as highly specialized organs in airway protection, respiration and phonation. Hbk Behav Neurosci. 2010; 19:13–21.10.1016/B978-0-12-374593-4.00002-4

Kirkwood PA. On the use and interpretation of cross-correlations measurements in the mammalian central nervous system. J Neurosci Methods. 1979; 1(2):107–132. [PubMed: 161793]

Krolo M, Stuth EA, Tonkovic-Capin M, Dogas Z, Hopp FA, McCrimmon DR, Zuperku EJ. Differential roles of ionotropic glutamate receptors in canine medullary inspiratory neurons of the ventral respiratory group. J Neurophysiol. 1999; 82(1):60–68. [PubMed: 10400935]

Lindsey BG, Rybak IA, Smith JC. Computational models and emergent properties of respiratory neural networks. Compr Physiol. 2012; 2(3):1619–1670.10.1002/cphy.c110016 [PubMed: 23687564]

Ludlow CL. Central nervous system control of interactions between vocalization and respiration in mammals. Head Neck. 2011; 33(Suppl 1):S21–25.10.1002/hed.21904 [PubMed: 21901780]

Lumsden T. Observations on the respiratory centres in the cat. J Physiol London. 1923; 57:153–160. [PubMed: 16993609]

MacDonald SM, Tin C, Song G, Poon CS. Use-dependent learning and memory of the Hering-Breuer inflation reflex in rats. Exp Physiol. 2009; 94(2):269–278.10.1113/expphysiol.2008.045344 [PubMed: 19028808]

Maltby A, Jones KE, Jones G. Understanding the evolutionary origin and diversification of bat echolocation calls. Hbk Behav Neurosci. 2010; 19:37–47.10.1016/B978-0-12-374593-4.0005-X

Martin RJ, Wilson CG. Apnea of prematurity. Compr Physiol. 2012; 2(4):2923–2931.10.1002/cphy.c100021 [PubMed: 23720269]

Molkov YI, Bacak BJ, Dick TE, Rybak IA. Control of breathing by interacting pontine and pulmonary feedback loops. Front Neural Circuits. 2013; 7:16.10.3389/fncir.2013.00016 [PubMed: 23408512]

Ostojic S, Brunel N, Hakim V. How connectivity, background activity, and synaptic properties shape the cross-correlation between spike trains. J Neurosci. 2009; 29(33):10234–10253.10.1523/JNEUROSCI.1275-09.2009 [PubMed: 19692598]

Paxinos, G.; Carrive, P.; Wang, H.; Wang, P. Chemoarchitectonic atlas of the rat brainstem. Academic Press; San Diego: 1999.

Paxinos, G.; Watson, C. The Rat Brain in Stereotaxic Coordinates. second edition. Academic Press; San Diego: 1986.

Pernice V, Staude B, Cardanobile S, Rotter S. How structure determines correlations in neuronal networks. PLoS Comput Biol. 2011; 7(5):e1002059.10.1371/journal.pcbi.1002059 [PubMed: 21625580]

Pitts T. Airway protective mechanisms. Lung. 201310.1007/s00408-013-9540-y

Poon CS, Song G. Bidirectional plasticity of pontine pneumotaxic postinspiratory drive: implication for a pontomedullary respiratory central pattern generator. Prog Brain Res. 2014; 209:235–254.10.1016/B978-0-444-63274-6.00012-6 [PubMed: 24746051]

Richter DW, Ballanyi K, Schwarzacher S. Mechanisms of respiratory rhythm generation. Curr Opin Neurobiol. 1992; 2(6):788–793. [PubMed: 1362108]

Segers LS, Nuding SC, Dick TE, Shannon R, Baekey DM, Solomon IC, Morris KF, Lindsey BG. Functional connectivity in the pontomedullary respiratory network. J Neurophysiol. 2008; 100(4):1749–1769.10.1152/jn.90414.2008 [PubMed: 18632881]

Segers LS, Shannon R, Lindsey BG. Interactions between rostral pontine and ventral medullary respiratory neurons. J Neurophysiol. 1985; 54(2):318–334. [PubMed: 4031991]

Shevtsova NA, Manzke T, Molkov YI, Bischoff A, Smith JC, Rybak IA, Richter DW. Computational modelling of 5-HT receptor-mediated reorganization of the brainstem respiratory network. Eur J Neurosci. 2011; 34(8):1276–1291.10.1111/j.1460-9568.2011.07825.x [PubMed: 21899601]

Shiba, K. Functions of larynx in breathing, vocalization and airway protective reflexes. In: Brudzynski, SM., editor. Handbook of Mammalian Vocalization: An Integrative Neuroscience Approach, Handbook of Behavioral Neuroscience. Vol. 19. Elsevier Science Bv; Amsterdam: 2010. p. 373-381.

Siniaia MS, Young DL, Poon CS. Habituation and desensitization of the Hering-Breuer reflex in rat. J Physiol. 2000; 523(Pt 2):479–491. [PubMed: 10699090]

Smith JC, Abdala AP, Borgmann A, Rybak IA, Paton JF. Brainstem respiratory networks: building blocks and microcircuits. Trends Neurosci. 2013; 36(3):152–162.10.1016/j.tins.2012.11.004 [PubMed: 23254296]

Smith JC, Abdala AP, Koizumi H, Rybak IA, Paton JF. Spatial and functional architecture of the mammalian brain stem respiratory network: a hierarchy of three oscillatory mechanisms. J Neurophysiol. 2007; 98(6):3370–3387. [PubMed: 17913982]

Smotherman M, Kobayasi K, Ma J, Zhang S, Metzner W. A mechanism for vocal-respiratory coupling in the mammalian parabrachial nucleus. J Neurosci. 2006; 26(18):4860–4869.10.1523/JNEUROSCI.4607-05.2006 [PubMed: 16672660]

Smotherman, M.; Schwartz, C.; Metzner, W. Vocal-respiratory interactions in the parabrachial nucleus. In: Brudzynski, SM., editor. Handbook of Mammalian Vocalization: An Integrative

Neuroscience Approach, Handbook of Behavioral Neuroscience. Vol. 19. Elsevier Science Bv; Amsterdam: 2010. p. 383-392.

Smotherman M, Zhang S, Metzner W. A neural basis for auditory feedback control of vocal pitch. J Neurosci. 2003; 23(4):1464–1477. [PubMed: 12598635]

Song G, Poon C. Lateral parabrachial nucleus mediates shortening of expiration during hypoxia. Respir Physiol Neurobiol. 2009; 165(1):1–8. [PubMed: 18992853]

Song G, Tin C, Giacometti E, Poon CS. Habituation without NMDA receptor-dependent desensitization of Hering-Breuer apnea reflex in a *Mecp2*$^{+/-}$ mutant mouse model of Rett Syndrome. Front Integr Neurosci. 2011; 5:6.10.3389/fnint.2011.00006 [PubMed: 21629824]

Song G, Wang H, Xu H, Poon CS. Kolliker-Fuse neurons send collateral projections to multiple hypoxia-activated and nonactivated structures in rat brainstem and spinal cord. Brain Struct Funct. 2012; 217(4):835–858.10.1007/s00429-012-0384-7

Song G, Yu Y, Poon CS. Cytoarchitecture of pneumotaxic integration of respiratory and nonrespiratory information in the rat. J Neurosci. 2006; 26(1):300–310.10.1523/JNEUROSCI.3029-05.2006 [PubMed: 16399700]

Stettner GM, Huppke P, Brendel C, Richter DW, Gartner J, Dutschmann M. Breathing dysfunctions associated with impaired control of postinspiratory activity in Mecp2-/y knockout mice. The Journal of physiology. 2007; 579(Pt 3):863–876. [PubMed: 17204503]

Stettner GM, Zanella S, Huppke P, Gartner J, Hilaire G, Dutschmann M. Spontaneous central apneas occur in the C57BL/6J mouse strain. Respir Physiol Neurobiol. 2008; 160(1):21–27.10.1016/j.resp.2007.07.011 [PubMed: 17869191]

Subramanian HH. Descending control of the respiratory neuronal network by the midbrain periaqueductal grey in the rat in vivo. The Journal of physiology. 2013; 591(Pt 1):109–122.10.1113/jphysiol.2012.24521 [PubMed: 23129795]

te Pas AB, Wong C, Kamlin CO, Dawson JA, Morley CJ, Davis PG. Breathing patterns in preterm and term infants immediately after birth. Pediatr Res. 2009; 65(3):352–356.10.1203/PDR.0b013e318193f117 [PubMed: 19391251]

Trousdale J, Hu Y, Shea-Brown E, Josic K. Impact of network structure and cellular response on spike time correlations. PLoS Comput Biol. 2012; 8(3):e1002408.10.1371/journal.pcbi.1002408 [PubMed: 22457608]

von Euler C. The functional organization of the respiratory phase-switching mechanisms. Fed Proc. 1977; 36(10):2375–2380. [PubMed: 892008]

Wang H, Zhang H, Song G, Poon CS. Modulation of Hering-Breuer reflex by ventrolateral pons. Adv Exp Med Biol. 2008; 605:387–392.10.1007/978-0-387-73693-8_68 [PubMed: 18085305]

Weese-Mayer DE, Lieske SP, Boothby CM, Kenny AS, Bennett HL, Silvestri JM, Ramirez JM. Autonomic nervous system dysregulation: breathing and heart rate perturbation during wakefulness in young girls with Rett syndrome. Pediatr Res. 2006; 60(4):443–449.10.1203/01.pdr.0000238302.84552.d0 [PubMed: 16940240]

Yizhar O, Fenno LE, Davidson TJ, Mogri M, Deisseroth K. Optogenetics in neural systems. Neuron. 2011; 71(1):9–34.10.1016/j.neuron.2011.06.004 [PubMed: 21745635]

Yokota S, Niu JG, Tsumori T, Oka T, Yasui Y. Glutamatergic Kolliker-Fuse nucleus neurons innervate hypoglossal motoneurons whose axons form the medial (protruder) branch of the hypoglossal nerve in the rat. Brain Res. 2011; 1404:10–20.10.1016/j.brainres.2011.06.025 [PubMed: 21724177]

Yokota S, Oka T, Tsumori T, Nakamura S, Yasui Y. Glutamatergic neurons in the Kolliker-Fuse nucleus project to the rostral ventral respiratory group and phrenic nucleus: a combined retrograde tracing and in situ hybridization study in the rat. Neurosci Res. 2007; 59(3):341–346.10.1016/j.neures.2007.08.004 [PubMed: 17888537]

Yokota S, Tsumori T, Ono K, Yasui Y. Glutamatergic pathways from the Kolliker-Fuse nucleus to the phrenic nucleus in the rat. Brain Res. 2004; 995(1):118–130. [PubMed: 14644477]

Zhou Z, Champagnat J, Poon CS. Phasic and long-term depression in brainstem nucleus tractus solitarius neurons: differing roles of AMPA receptor desensitization. J Neurosci. 1997; 17(14):5349–5356. [PubMed: 9204919]

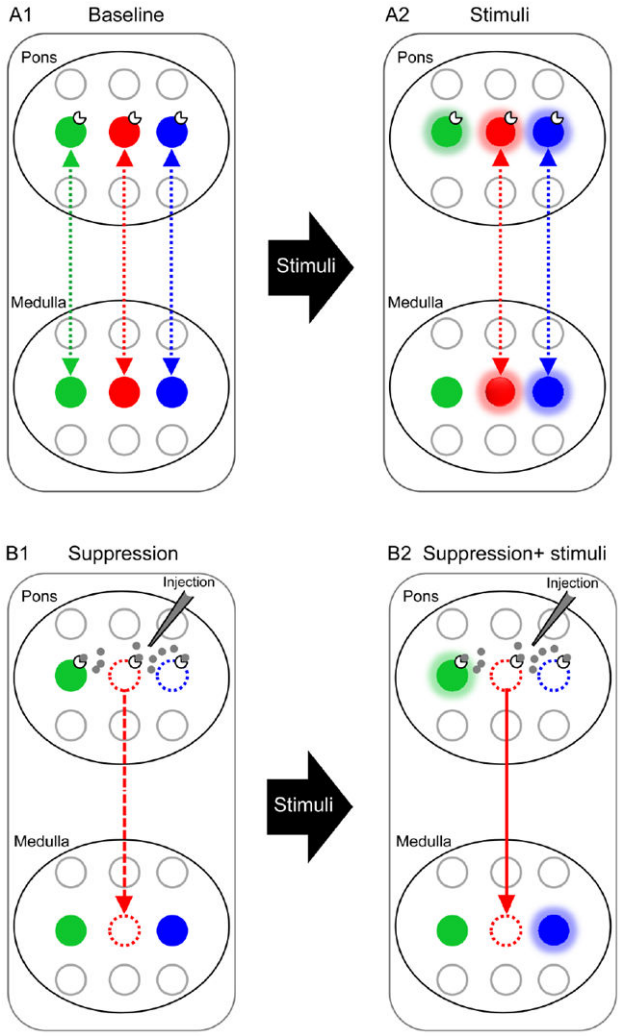

Figure 1.

Schematic illustration of the multiscale temporal-cellular coincident fingerprinting assay for long-range functional connectivity mapping. **A1:** Pairs of neuronal pools in separate brain nuclei (pons and medulla) are potentially functionally connected either way (broken bidirectional arrows) if their discharge patterns in quiescent state (baseline) contain timing-specific components that are temporally correlated to one another. Distinct timing-specific correlated discharge patterns are denoted by different colors (green, red, blue). Non-correlated components are uninformative and are excluded from analysis. **A2:** Functional connectivity from the green pontine pool to green medullary pool cannot be ascertained if the former is excited by stimuli but not the latter. **B1.** To investigate whether the timing-specific and response-specific correlations among the remaining red and blue neuronal pools in pons and medullar signify functional connectivity, corresponding neuronal pools in pons are suppressed (broken open circles) by cell-specific pharmacological or other blockers. In this example, the red neuronal pool in medulla is said to likely receive excitatory drive (broken downward arrow) from its counterpart in pons, since its activity is attenuated or silenced by suppression of the latter. The same cannot be said of the blue neuronal pools,

however, since the blue neuronal pool in medulla remains active after its counterpart in pons is suppressed. **B2.** Excitatory connectivity from red pontine pool to red medullary pool as determined in B1 is confirmed (solid downward arrow) if the response of the red medullary pool to afferent stimulation is abolished after suppression of the red pontine pool. Together, these timing-specific, response-specific, and cell-specific properties constitute a set of temporal-cellular coincident 'fingerprint markers' that unequivocally establish excitatory connectivity of the red neuronal pool in pons to that in medulla—in a manner analogous to fingerprint matching. The methods of stimulation and suppression of neuronal activity may vary depending on the cellular properties of the neuronal populations of interest but the set of temporal-cellular markers should be chosen to uniquely verify neuronal connectivity. Inhibitory connectivity between neuronal pools whose discharge patterns are anti-synchronized may also be discerned in a similar fashion. For the assay as depicted above, possible functional connectivity from medullary pools to corresponding pontine pools cannot be ruled out and must be tested separately. In this study, temporal-cellular coincident fingerprint markers are provided by a set of neuronal characteristics including post-I phase specificity, hypoxia-induced short-term potentiation, and critical dependence on NMDAR activity of the pontine pneumotaxic mechanism as manifested at the systems, network, and cellular levels, as demonstrated in Figs. 2-6 below. Note that the long-range functional connectivity so determined could be either monosynaptic or oligosynaptic, hence additional tests (such as demonstrated in Fig. 3E) are necessary to address this issue.

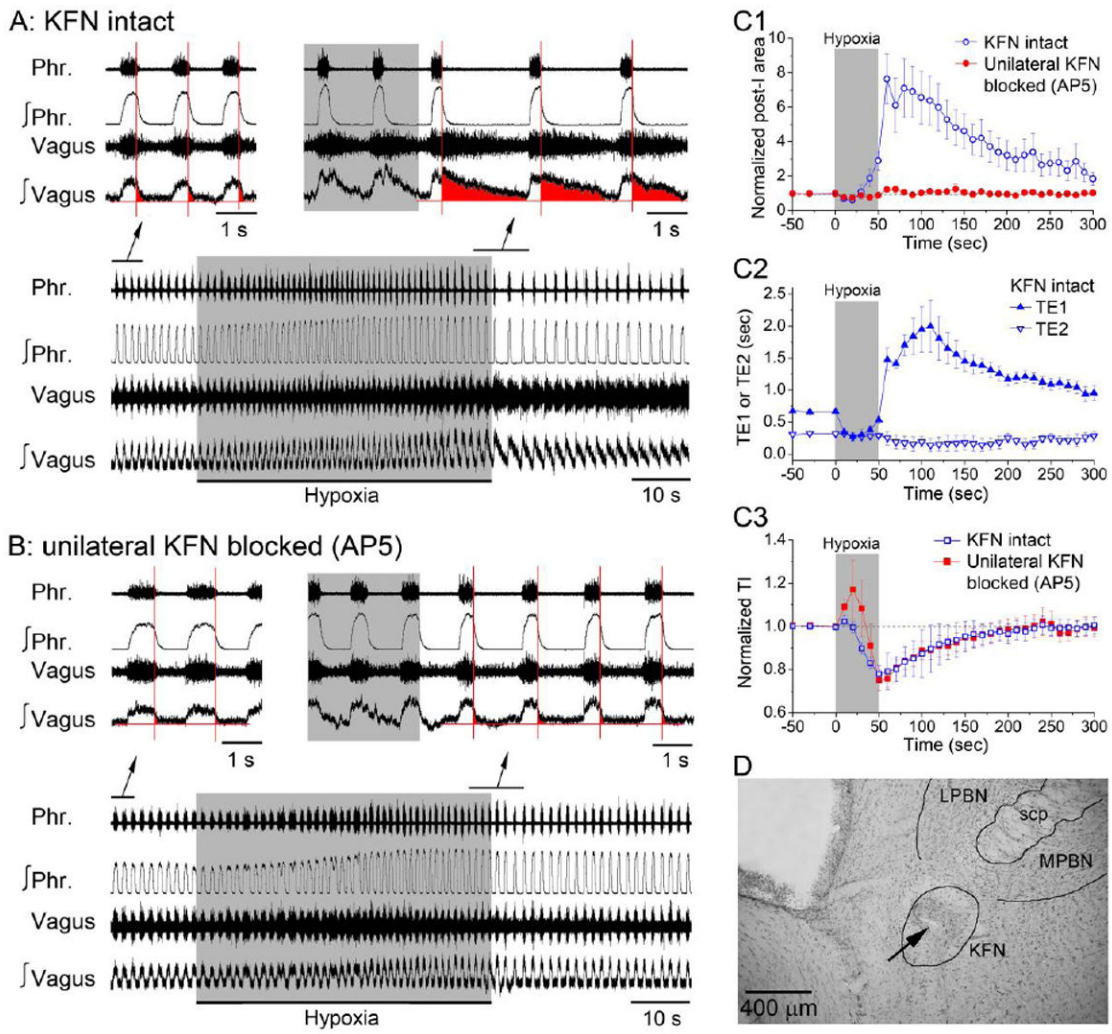

Figure 2. Temporal-cellular coincident fingerprinting of post-I pathway at systems level

A:Timing-specific and response-specific markers of the post-I pathway as seen at the systems level from vagal-laryngeal post-I motor activity in rats. Post-I activity (red shaded area of integrated vagal-laryngeal motor activity in insets) was markedly increased after hypoxic stimulation indicating STP. Vertical red lines indicate onset of post-I phase as indicated by end of phrenic motor activity and onset of vagal-laryngeal post-I motor activity.

B: Cell-specific marker of the post-I pathway as seen at the systems level from the suppression of vagal-laryngeal post-I motor activity and abolition of its STP after microinjection of NMDAR antagonist AP5 into KFN.

C: Summary of all timing-specific, response-specific and cell-specific markers of the post-I pathway at the systems level (panel C1) as revealed by the post-hypoxic STP of vagal-laryngeal post-I motor activity (area of integrated vagal-laryngeal motor activity) and its abolition after microinjection of AP5 into KFN. Panels C2 and C3: Post-hypoxic STP and its abolition by NMDAR blockade was specific to the post-I phase (duration T_{E1}) and not the late-expiratory phase (duration T_E2) or inspiratory phase (duration T_I). Data are means ± SE (n = 5).

D: Photo of microinjection site in intermediate KFN. *Arrow* indicates the lesion. LPBN, lateral parabrachial nucleus; MPBN, medial parabrachial nucleus; scp, superior cerebellum peduncle; 5, trigeminal motor nucleus.

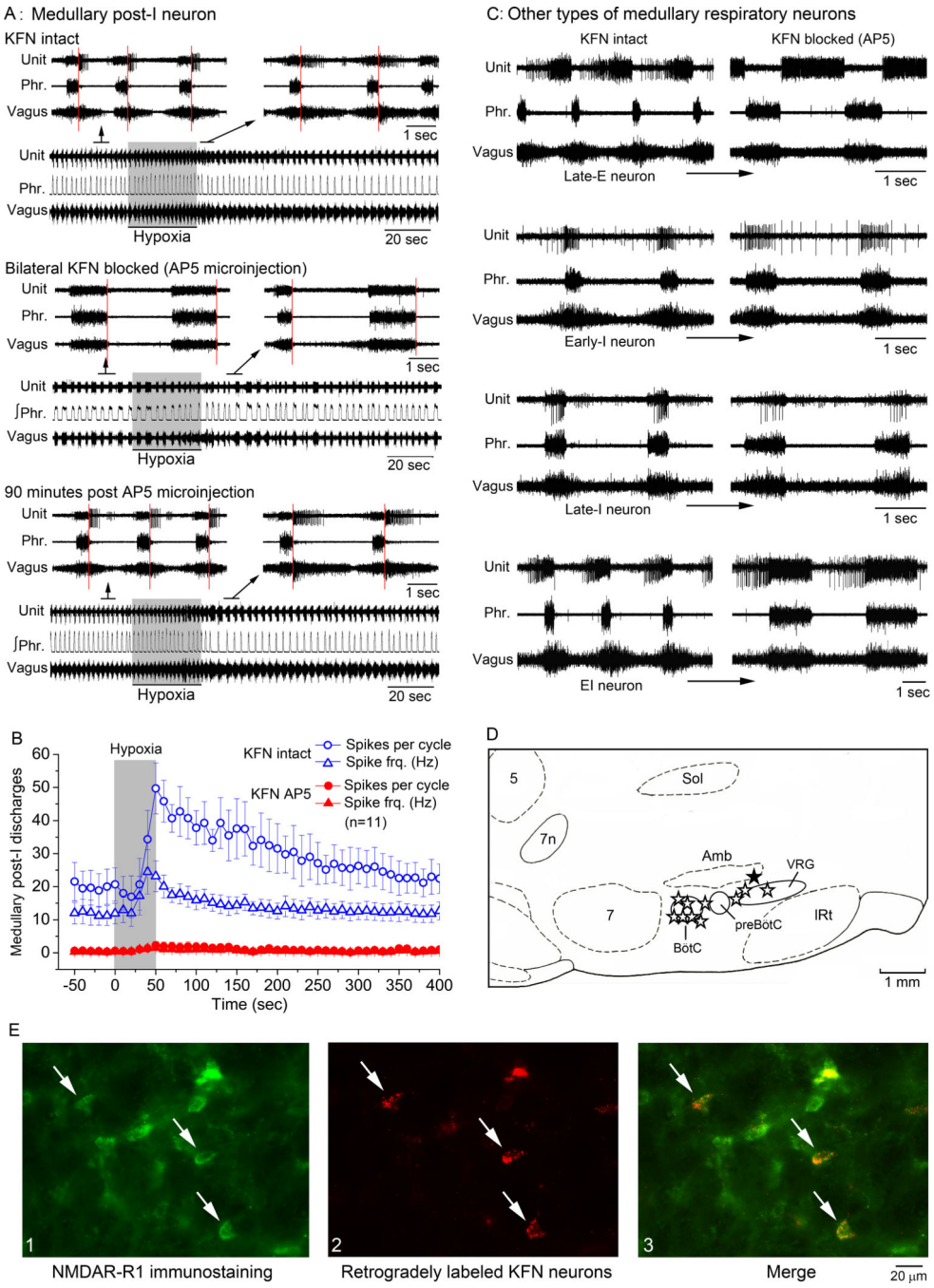

Figure 3. Temporal-cellular coincident fingerprinting of post-I pathway at network level

Similar timing-specific, response-specific and cell-specific markers of the post-I pathway seen at the systems level were also expressed in medullary post-I neurons at the network level.

A: Microinjection of AP5 into KFN markedly suppressed medullary post-I neuron activity (recorded from the Bötzinger complex) and abolished its STP induced by hypoxic stimulus.

B: Summary effects in 11 medullary post-I neurons demonstrating post-hypoxic STP in both firing frequency and number of spikes per cycle, and the abolition of such STP after microinjection of AP5 into KFN.

C: These timing-specific, response-specific and cell-specific effects were not seen in other respiratory-related neurons in medulla indicating that the corresponding markers were specific to the post-I pathway.

D: Loci of the recorded medullary post-I neurons plotted onto a sagittal medullary plane at 1.9 mm lateral from midline. The filled star indicates a post-I motoneuron that was antidromically activated by vagal stimulation. BötC, Bötzinger complex; preBötC, preBötzinger complex; VRG, ventral respiratory group; Amb, ambiguous nucleus; Sol, solitary tract; 5, trigeminal motor nucleus; 7, facial nucleus; 7n, facial nerve; lRt, lateral reticular nucleus.

E: Expression of NMDAR-R1 subunit (NR1) by KFN neurons that projected to the Bötzinger complex (BötC). Photo 1: NR1-expressing KFN neurons as visualized using immunofluorescent staining (*arrows*). Photo 2: Retrogradely labeled neurons (*arrows*) in KFN as revealed by retrograde tracer RetroBeads™ microinjected into BötC. Photo 3: Merging of photo 1 and photo 2, showing neurons that were double-labeled (*arrows*). In control sections that were processed with the same method but without the anti-NR1 antibody, no neuron was labeled for NR1 (data not shown).

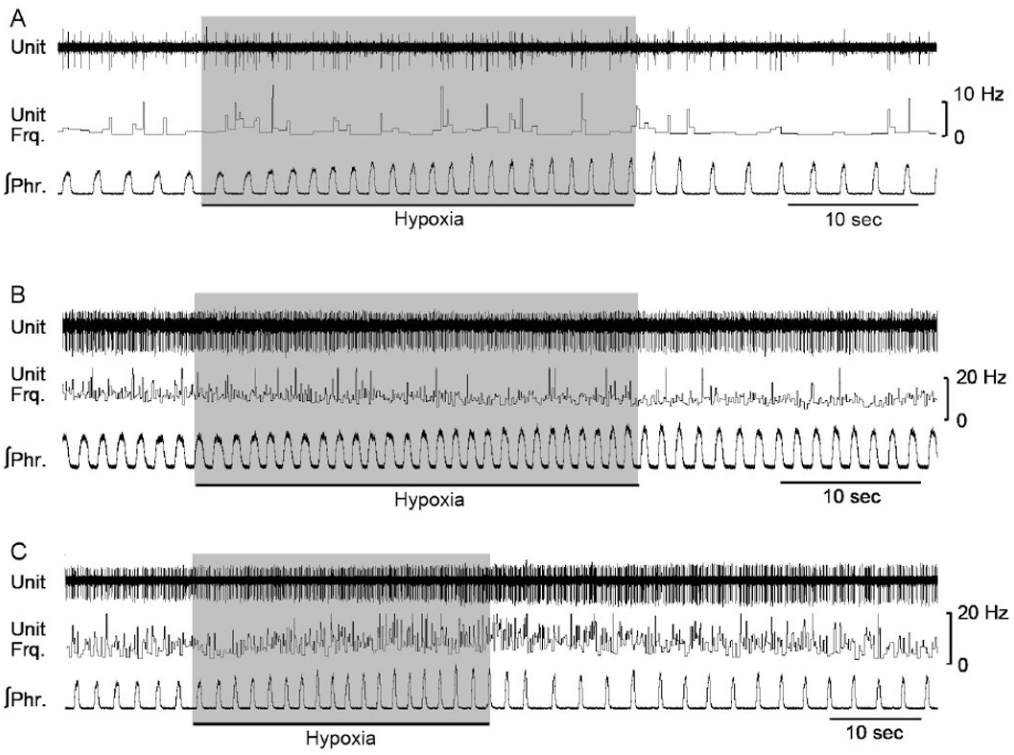

Fig. 4.

Tonic neurons in KFN did not exhibit hypoxia-induced STP that was characteristic of the pontomedullary post-I pathway. Indeed, none of the tonic neurons recorded from KFN (n = 46) were responsive to hypoxic stimulus, as seen here in three representative neurons.

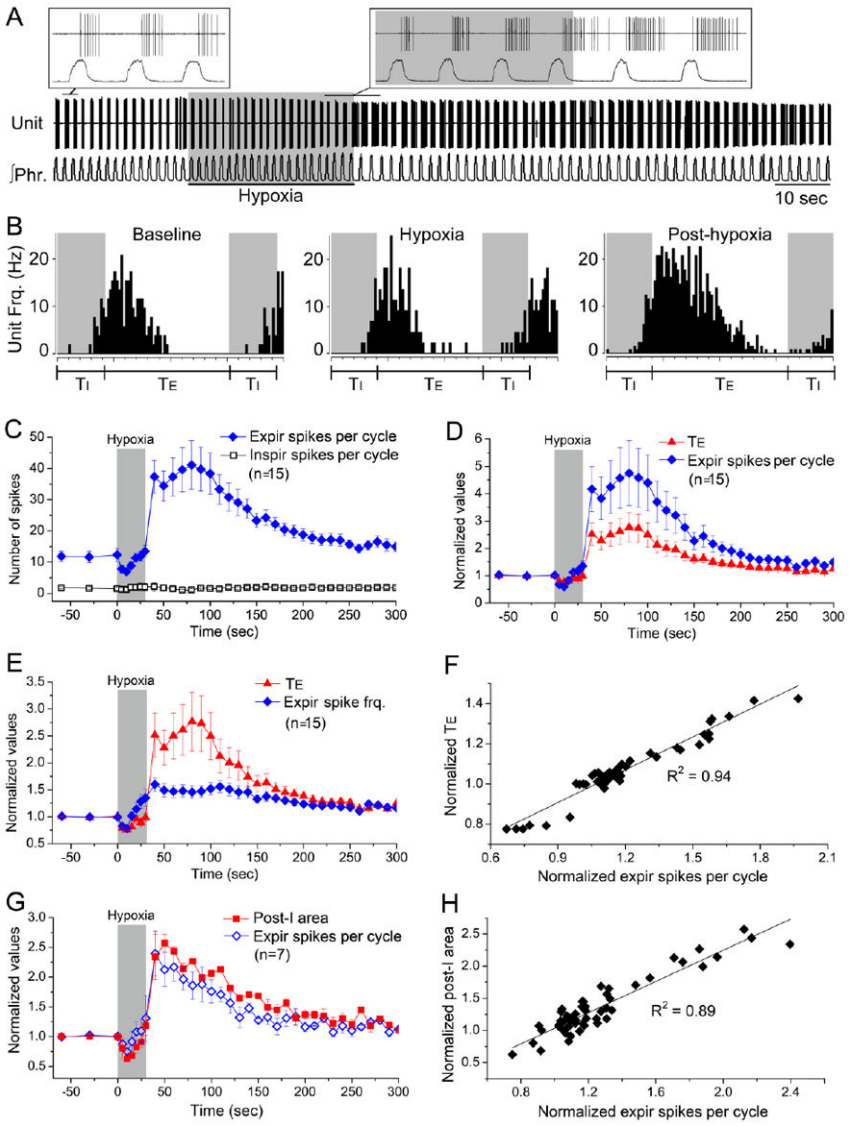

Figure 5. Temporal-cellular coincident fingerprinting of post-I pathway at cellular level: timing-specific and response-specific markers

Similar timing-specific and response-specific markers of the post-I pathway seen at the systems and network levels were also expressed in KFN early-E neurons at the cellular level.

A: Representative early-E neuron discharge recorded from KFN. Under control condition, this neuron started firing at inspiratory-expiratory phase transition (with 1-2 spikes in late inspiratory phase in some cycles) and continued firing with a decrementing pattern until mid-expiration. Hypoxia caused strong post-hypoxia potentiation in this neuron.

B: Perievent histograms showing that unit discharge duration was reduced during hypoxia and increased during the post-hypoxia period. In contrast, peak discharge frequency was not decreased during hypoxia and was increased during the post-hypoxia period.

C: Summary of 15 KFN early-E neurons. Most KFN early-E neurons discharged a few spikes during late inspiration before reaching peak discharge frequency at inspiratory-

expiratory phase transition with ensuing decrementing discharge pattern until mid-expiration. Hypoxia potentiated their expiratory discharges (spikes/cycle) but had no effect on their inspiratory discharges.

D-F: The expiratory discharges and mean expiratory firing frequencies (spikes/cycle divided by expiratory duration) of KFN early-E neurons (n=15) correlated directly with expiratory duration (T_E) during hypoxia and post-hypoxia periods.

G-H: In another series of experiment, the discharges of KFN early-E neurons (n=7) were found to correlate directly with ∫vagal post-I area during hypoxia and post-hypoxia periods.

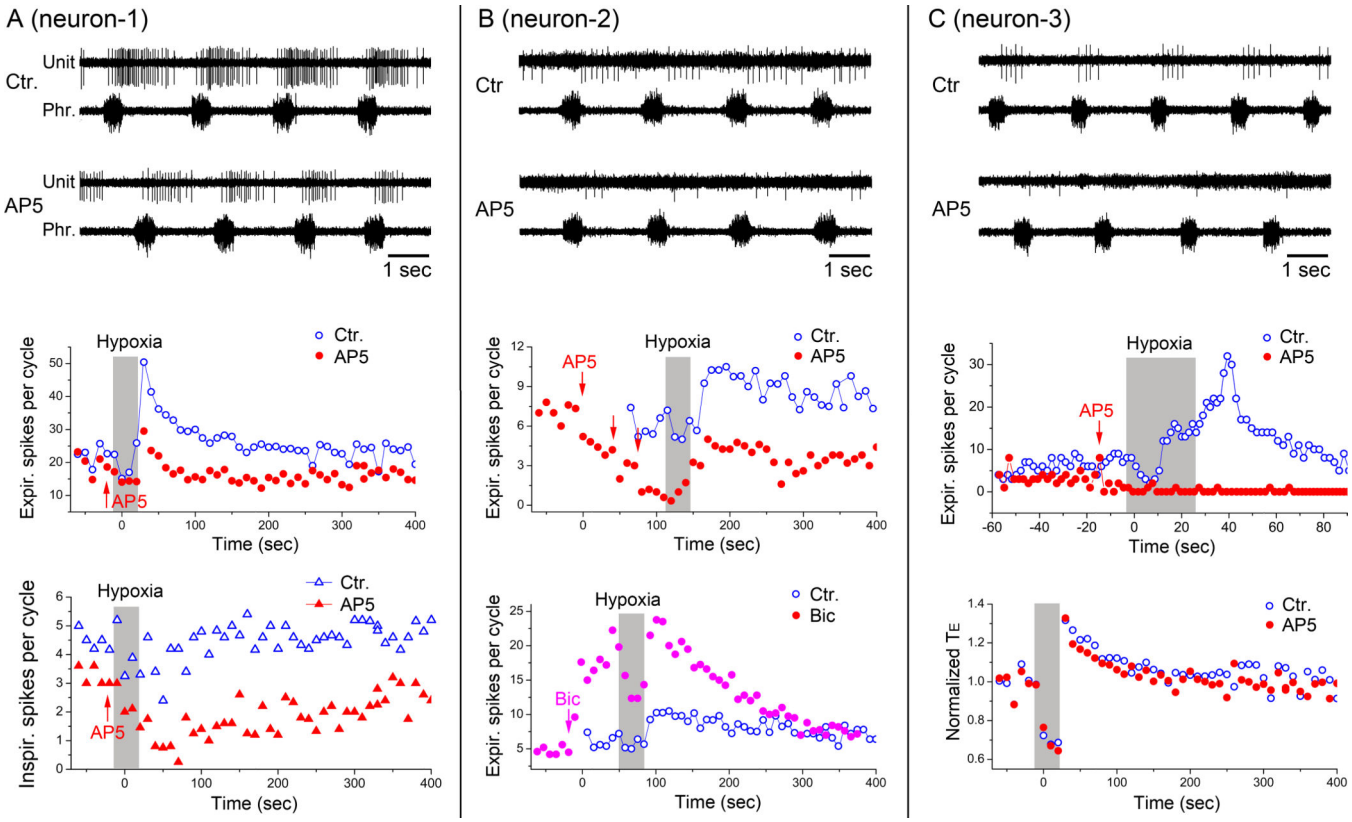

Figure 6. Temporal-cellular coincident fingerprinting of post-I pathway at cellular level: cell-specific marker

Similar cell-specific marker of the post-I pathway seen at the systems and network levels was also expressed in KFN early-E neurons at the cellular level.

A: *Upper panel:* Discharge of a KFN early-E neuron (neuron-1) relative to phrenic discharge before and after AP5 picoinjection. Under baseline condition this neuron discharged predominantly in early-E/post-I phase (20-30 spikes) but also a few spikes (3-7 spikes) in inspiratory phase. *Mid panel:* The early-E discharge of this unit was slightly depressed after picoinjection of AP5. Immediately after the injection, hypoxia evoked a much smaller post-hypoxic STP. *Bottom panel:* The inspiratory discharge of this unit was not significantly affected by hypoxia but was depressed by picoinjection of AP5.

B: *Upper panel:* Neuron-2 discharged only during early-E phase. *Mid panel:* This unit was almost completely depressed after repeated picoinjections (3x) of AP5. Post-hypoxic STP was greatly reduced. *Bottom panel:* In contrast, after unit 2 completely recovered from injections of AP5, picoinjection of bicuculline caused excitation of this unit. Hypoxia still caused acute depression of the unit discharge but the post-hypoxic STP was much smaller.

C: *Upper panel:* Neuron-3 discharged predominantly during early-E phase. *Mid panel:* This unit was almost completely silenced after local picoinjection of AP5, and post-hypoxic STP was abolished. *Bottom panel:* Local picoinjection of AP5 at a single KFN early-E neuron did not affect overall hypoxic response in expiratory duration (T_E).